Image-Based Conductivity and Permittivity Mapping with RF Receiver Arrays

Seung-Kyun Lee[1], Selaka Bandara Bulumulla[1], and Ileana Hancu[1]
[1]*GE Global Research, Niskayuna, NY, United States*

Target Audience: Researchers interested in MR-based tissue electrical property mapping and novel image contrast

Introduction: It was recently proposed that tissue electrical properties (TEP) can be calculated from RF-induced complex image intensity variation in standard MR images, without B_1 mapping [1]. An additional advantage of the method is that the images can be obtained with a receiver array, as is most common in body scans. This is in contrast with a more widely used, B_1 mapping based method [2,3], where a switched mode birdcage-type coil is required for RF transmission and reception. We demonstrate here image-based TEP mapping with a receiver array using a zero-TE low flip angle gradient echo (ZTE) sequence, and evaluate the performance of this approach in phantoms.

Theory: The principle of the image-based TEP mapping is outlined in [1]. The central equations (Eqs. 1-2) are based on two assumptions: the length scale of B_1^+ and B_1^- variation is determined by the wave vector k of RF in tissue, and B_1^+ and B_1^- maps are similar to each other (within a constant factor). The former implies that the RF distribution in the image is dominated by tissue-RF interaction, as opposed to factors such as coil geometry. The advantage of this formulation is that the error due to mismatch between B_1^+ and B_1^- grows quadratically with the mismatch, as opposed to linearly as in the conventional, B_1 map and phase approximation-based [2,3] method. If a phased array is used for imaging, Eqs. (1-2) can still be used if B_1^- is replaced by the combined receiver field map which is a linear combination of individual, complex coil sensitivity maps, $B_1^- = c_1 B_1^{-(1)} + c_2 B_1^{-(2)} + \cdots + c_N B_1^{-(N)}$. In this case, the combined B_1^- map should satisfy the RF distribution requirements, namely the dominance of tissue-RF interaction and similarity to B_1^+. Note that combined image variation being dominated by tissue-RF interaction is a common requirement for phased-array imaging.

$$\epsilon_r \approx -\frac{1}{\mu\epsilon_0\omega^2} Re\left(\frac{\nabla^2\sqrt{B_1^+B_1^-}}{\sqrt{B_1^+B_1^-}}\right) \quad (1)$$

$$\sigma \approx \frac{1}{\mu\omega} Im\left(\frac{\nabla^2\sqrt{B_1^+B_1^-}}{\sqrt{B_1^+B_1^-}}\right) \quad (2)$$

Figure 1. Equations for image based TEP mapping

Method		Label
B_1 map-based, head T/R		A
Image-based (ZTE)	head T/R	B
	body T/R	C
	body Tx, 8ch Rx (uniform weight)	D
	body Tx, 8ch Rx (optimized weight)	E

Table 1. Five methods used for the phantom experiment

Methods: All imaging was done with Discovery 3.0 T MR750 (GE Healthcare, Waukesha, WI). For the phantom experiment, three water/salt based cylindrical phantoms of conductivities 0.08,046 and 0.92 S/m were used. Five sets of acquisitions, as described in Table 1, were made. The first acquisition (Method A) defined the reference method, and entailed B_1^+ mapping and spin echo imaging with a standard head T/R coil. In the four ZTE acquisitions, various coils were used for comparison. ZTE imaging implemented a sequence with 3D radial center-out trajectory, in a manner similar to [4]. Total acquisition time was 15 min for Method A, and 27 sec for Methods B-E. An eight-channel, receive-only brain coil (GE Healthcare) was used for the last two methods. The coil data were combined with no weight (Method D) or with complex phase weights that maximized the minimum intensity of the combined image (Method E), according to $\vec{c} = argmin_{\vec{c}}\, 1/\min(\|c_1 I_1 + c_2 I_2 + \cdots + c_N I_N\|^2)$, where $|c_1| = |c_2| = \cdots = 1$.

Results and Discussion: Figure 2 (a) compares electrical property maps of the phantom obtained from different methods. The pixel statistics (mean ± stdev) for each cylinder are shown graphically in Fig. 2(b). When the same head T/R coil was used, ZTE and B_1^+ mapping based methods performed equally well, highlighting the speed advantage of the former. Methods C-E demonstrated the potential for the image-based method for a body scan. Poor SNR in body T/R coil acquisition resulted in very noisy electrical property maps in Method C, whereas the phased array acquisitions (D, E) produced results similar to the reference method (A). In this test with a brain array, where coil elements are roughly symmetrically placed around the phantom, optimizing coil combination weights made only minor difference in the image itself (not shown) and the reconstructed electrical property maps. Proper coil combination is expected to be more important in torso or breast scans with irregularly positioned coil elements [5].

Conclusion: We have shown that image based TEP calculation can be applied to images acquired with a receiver array. The reconstruction algorithm is the same as in the single T/R coil case. The proposed method demonstrated faster TEP mapping and potential for improved accuracy with the use of a receiver array, which could be particularly useful for body scans.

Acknowledgement: This work was supported by the NIH grant 1R01CA154433.

References: [1] Lee S-K et al, ISMRM 2013, 462 [2] Katscher U. et al, IEEE Trans Med Imaging 28:1365 (2009) [3] Bulumulla S.B. et al, Concepts Magn Reson 41:13 (2012) [4] Madio et al. MRM 34:525 (1995) [5] Shin J et al. ISMRM 2013, 4180

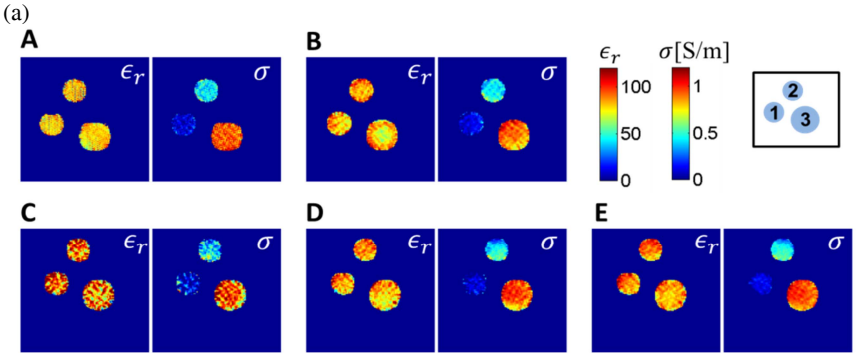

Figure 2. (a) Permittivity and conductivity maps of the phantom for the five methods of Table 1. The cylinders 1-3 had diameters of 7.7 cm, 7.7 cm, 9.4 cm, respectively. (b) Pixel average and standard deviation of electrical properties for the three cylinders. For each method, the three entries correspond to cylinders 1-3 (left-right). The horizontal lines are ground truth values from literature and dielectric probe data.